PRIFYSGOL
ABERYSTWYTH
UNIVERSITY

Aberystwyth University

Modeling subauroral polarization streams equatorward of the plasmapause footprints

Pintér, Balázs; Thom, S. D.; Balthazor, R. L.; Vo, H.; Bailey, G. J.

Modeling sub-auroral polarization streams equatorward of the plasmapause footprints

B. Pintér[1,2], S. D. Thom[1], R. Balthazor[1], H. Vo[3], and G. J. Bailey[1]

[1]Department of Applied Mathematics, The University of Sheffield, Sheffield, UK

[1]Institute of Mathematical and Physical Sciences, The University of Wales, Aberystwyth, UK

[2]Arecibo Observatory, Puerto Rico, USA

Abstract. We report on a modelling study on the effects of Sub-Auroral Polarization Stream (SAPS) events equatorward of the plasmapause footprints, using the Sheffield Coupled Thermosphere Ionosphere Plasmasphere model (CTIP). SAPS events are simulated by imposing a poleward electric field for two hours in the pre-midnight sector between $50°$ and $60°$ magnetic latitude. The presence of the SAPS results in a decrease in vertical total electron count (VTEC) and F-region ion density, whilst the height of the F-region can rise by up to 100 km. A study of the relative importance of the physical processes finds that the most significant contribution is the temperature increase due to ion-neutral friction, resulting in increased reaction rates of O^+ loss. The recovery time for the SAPS studied is up to 10 hours.

1. Introduction

The sub-auroral inner magnetosphere is a strongly coupled system where, during geomagnetically active periods, poleward directed electric fields are formed just equatorward of the diffuse aurora. The term Sub-Auroral Polarization Stream (SAPS) [Foster and Burke [2002]] is the name given to encompass the observations of various sub-auroral electric fields including polarization jets (PJs) [Galperin et al. [1973]], sub-auroral ion drift (SAID) [Smiddy et al. [1977]] and penetration electric fields [Yeh et al. [1991]].

Polarization jets (PJs) are narrow channels (less than $2°$ latitude) of intense westward plasma flows (500 m/s to >4 km/s), appearing near the polar wall of the ionosphere trough the evening sector. They were first discovered by the Kosmos-184 satellite [Galperin et al. [1973]]. Smiddy et al. [1977] also reported the observation of large subauroral electric fields. The term sub-auroral ion drift (SAID) was introduced by Spiro et al. [1979] and later used in the American literature for the same phenomenon (e.g. Anderson et al., 1991). Although the penetration electric fields reported by Yeh et al. [1991] are similar to PJ/SAID, they resulted in much broader regions of sunward plasma drift with large latitudinal extent and longer duration. While Anderson et al. [1991] associated SAID with only substorms, Burke et al. [2000] and Anderson et al. [2001] both showed that SAID can last throughout the main phase of geomagnetic storms.

There have been observations of large enhancements in the ionospheric ion temperature, upward vertical drifts, and depletions in the low-altitude ion density, associated with SAID. Enhanced temperatures due to increased ion-neutral friction have been shown to result in decreasing ionospheric O^+ and O_2^+ [Schunk et al. [1975]]. Modelling studies into the effects of large westward drifts imposed for 10 minutes on a closed tube of plasma at $L = 4$ resulted in enhanced ion temperatures and decreased F-region O^+ density [Sellek et al. [1991]; Sellek et al. [1992]]. However, observations made on the Atmospheric Explorer-C and Dynamics Explorer 2 spacecraft indicated that PJ/SAID events may last between 30 minutes and 3 hours [Anderson et al., 1991].

A model of SAID lasting 30 minutes showed increases in ion temperatures of over 3000 K at F region altitudes for ion drifts of 2 km/s [Moffett et al. [1992]]. The increased temperatures lasted the duration of the SAID. When the drift ceased, there was a rapid decrease of ion temperature as it returned to pre-event values. At 1000 km, the increase in ion temperature was 1000 K. The relative abundance of O^+ was also found to decrease during the SAID.

The average characteristics of SAPS events were reported by Foster and Vo [2002] using Millstone Hill ISR observations over two solar cycles (1979-2000). It was found that SAPS events in the pre-midnight sector lie equatorward of $L = 4$ (or magnetic latitude, $\lambda = 60°$), with latitudinal spans of $3-5°$ and with peak westward velocities of 1000 m/s for $Kp \approx 6$.

We present results from a modelling study of SAPS events in which the SAPS potential for each event is varied (-20, -40 and -60 kV) in the pre-midnight sector equatorward of the plasmapause footprints. The effects of the SAPS on the density and height of the ionospheric F-region and vertical total electron count (VTEC) are discussed.

2. Model Description

The Coupled Thermosphere-Ionosphere-Plasmasphere model (CTIP) was developed in collaboration between the University of Sheffield and University College, London and has been described in detail previously [Millward et al., 1996]. The plasmasphere model calculates time-dependent global, three-dimensional structure of the temperature, composition, velocity of the neutral atmosphere and density and velocity of the ions O^+, H^+ and He^+ by solving the nonlinear equations of continuity, momentum and energy. The density distributions of O_2^+, N_2^+ and NO^+ are calculated, assuming chemical equilibrium. The plasmasphere in the CTIP model has flux tubes arranged in 20 'groups' of 79 flux tubes positioned every $18°$ magnetic longitude. The plasmasphere extends from 80 km altitude up to about 28,700 km ($L = 4.5$).

The thermosphere code is a global, non-linear, time-dependent code originally developed at University College London (UCL) [Fuller-Rowell and Rees [1980]] and simulates the time-dependent structure of the wind vector, temperature and density of the neutral thermosphere by numerically solving the equations of momentum, energy and continuity. The thermosphere in the CTIP model is computed on
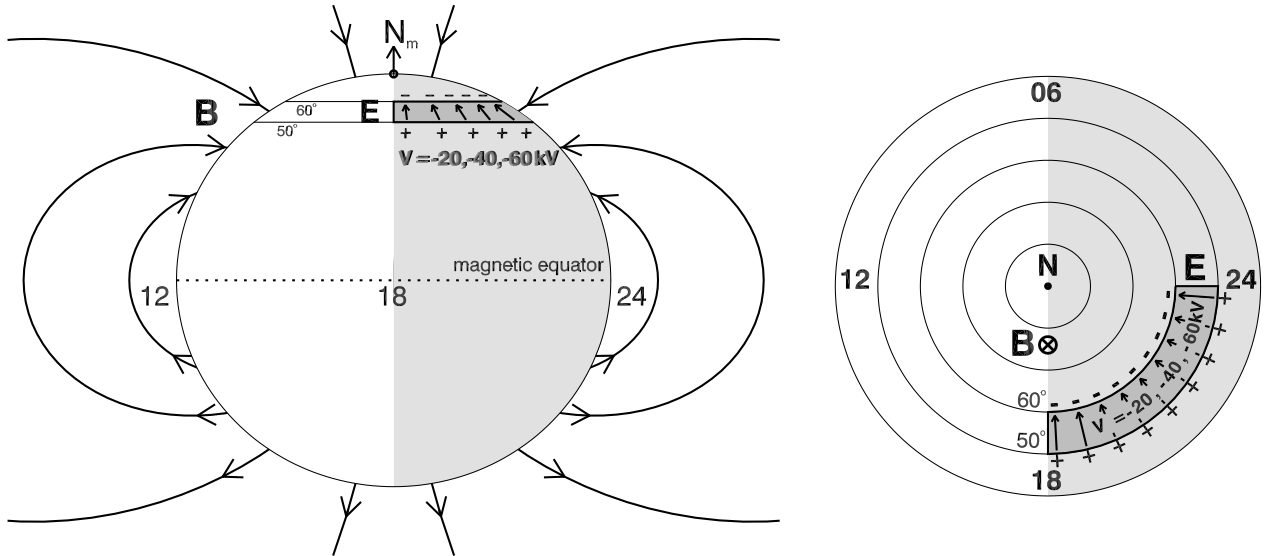
Figure 1. Schematic to illustrate the location of the northward-directed electric field responsible for a SAPS event in the CTIP model

grid points positioned globally every 2° latitude, 18° longitude and at 15 pressure level intervals vertically with a fixed lower pressure level at 1Pa/80 km. The pressure levels are separated by a distance equivalent to one scale height and cover the altitude region from 80 km, through the F-region peak, to around 350-500 km depending on the temperature.

The ion and electron temperatures are obtained using an extended Titheridge temperature model (TTM) [Webb and Essex, 2003], a modified version of the upper ionosphere and plasmasphere temperature model published by Titheridge [1998].

3. Model Inputs

The model was initially run for eight days in order to obtain a steady-state equilibrium (in a diurnal sense), for a northern hemisphere summer solstice conditions.
Following the work by Foster and Vo [2002] we simulate three SAPS events, corresponding to SAPS potentials of -20, -40 and -60 kV corresponding to $E \times B$ drift of 330, 670 and 1000 m/s, respectively. The three SAPS potentials also correspond to northward directed electric fields 18, 36 and 54 mV/m, respectively. They are imposed in the region between 18 and 24 MLT and $50° - 60° \lambda$. Our SAPS event is thus located in the pre-midnight sector, equatorward of the plasmapause footprints ($61.87° \lambda$ or $L = 4.5$) as seen in Figure 1.
We use a top-hat function for the spatial distribution of the SAPS potential because the grid resolutions of the CTIP coupled model are relatively coarse; in addition to the thermospheric grid described previously, the flux tube footprint spacings vary between one and five degrees latitude over the SAPS region, so reducing the spatial extent of the SAPS would risk introducing grid resolution problems. However, this paper restricts itself to discussing local (i.e., internal to the SAPS region) effects of the SAPS, rather than any neighbouring or far-field effects which would be more strongly related to the morphology of the imposed electric field. We accept that this is thus a limited study of SAPS with a larger than average (typically pseudo-Gaussian 3-5° half-width full maxima) spatial distribution, and must bear these caveats in mind when discussing the results. A future study with improved model resolution will allow us to investigate effects

of zonal, meridional, and temporal variations of the imposed SAPS.
During a SAPS event there is an increase in ion temperature attributed to ion-neutral frictional heating [Anderson et al. [1991]; Moffett et al. [1992]; Sellek et al. [1992]]. The extended TTM does not take into account the increase in ion temperatures due to ion-neutral frictional heating. Thus, an additional temperature profile based on work of [Moffett et al. [1992]; Sellek et al. [1992]] is included in order to simulate this heating. In Figure 2, the ion temperatures is calculated by the TTM (a), which is combined with the temperatures due to ion-neutral frictional heating (b), resulting in the total ion temperature (c) during a SAPS event. This ion-neutral friction is only included in the areas where SAPS occurs. The observational results are insufficient to provide an accurate correlation between the magnitude of the SAPS electric field and the resulting temperature increase due to ion friction. A parametric study on the SAPS effects with varying profiles of ion temperature increase will be the subject of a future study, but that is beyond the scope of this paper; her we use an additional ion temperature profile fixed for all values of SAPS potential, as given in Figure 2.

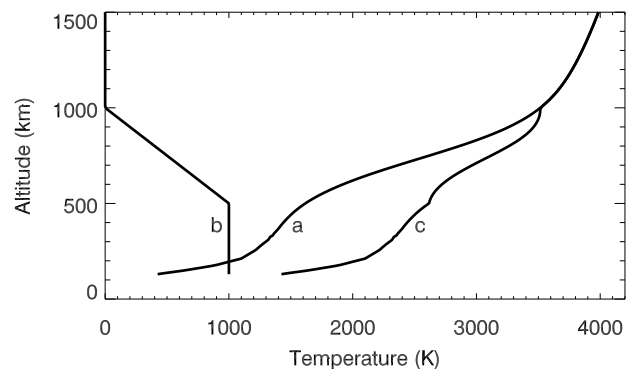

Figure 2. Ion temperatures in the mid-latitude ionosphere. a) Ion temperature given by the extended TTM, b) Extra temperature due to ion-neutral friction and c) TTM ion temperature including ion-neutral friction
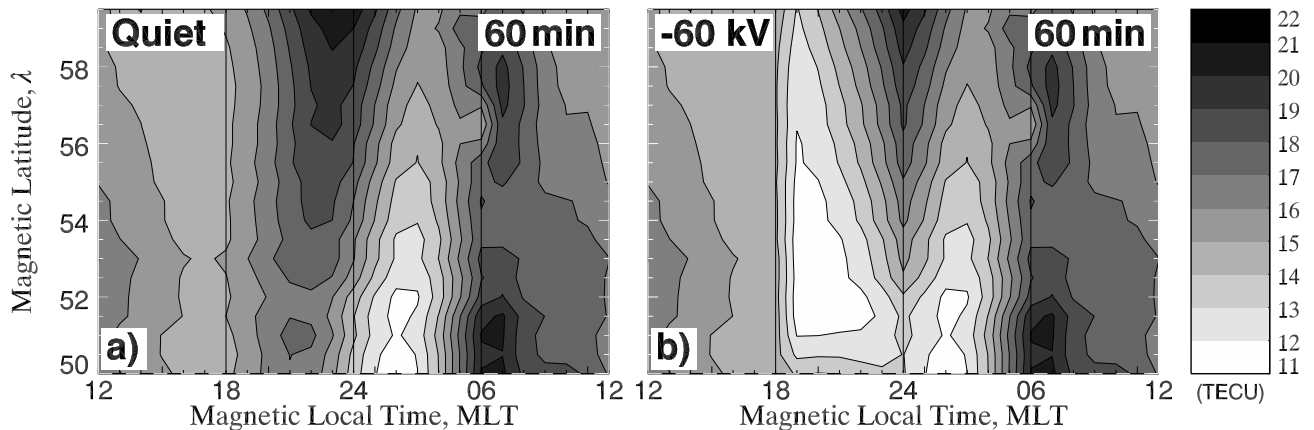
Figure 3. VTEC contour plot of a) a quiet time (0 kV) simulation and b) when a -60 kV potential is applied between 18 and 24 MLT and 50° to 60° magnetic latitude

The add-hoc value is constant 1000 K up to the altitude of 500 km, in accordance with Moffett et al. [1992], and it decreases linearly to 0 between 500 and 1000 km.

The modelled SAPS northward-directed electric field (corresponding to either -20, -40 or -60 kV) was started at 12 noon UT and remained constant for two hours, after which it was removed, and the model was run for a further 22 hours with the normal (SAPS-free) electric field.

4. Results and Discussion

Figure 3a is a contour plot for the vertical total electron count (VTEC) from 300 km to 800 km after a 60 min run of the quiet time (0 kV, i.e., no SAPS) simulation, as a function of MLT and magnetic latitude. VTEC is given in units of TECU, where 1 TECU is equivalent to 10^{16} electrons per m^2. We assume that the electron density is equal to the total ion density, which in the CTIP model is a combination of O^+, H^+, He^+, N_2^+ and O_2^+. Figure 3b shows the VTEC after a SAPS potential of -60 kV applied for 60 min . A significant decrease in VTEC is apparent between 18 and 24 MLT, where the SAPS electric field was applied between 50° to 60° magnetic latitude. The decrease of VTEC has a maximum at around 52°, which is somewhat lower than the middle of the latitudinal region embedded in the SAPS electric field. This 'latitudinal asymmetry' is probably due to the fact that 'latitudinal profile' of VTEC is asymmetric and has a minimum at around 52° for the quiet run, as can be seen in Figure 3a. The maximum percentage difference between the quiet time simulation and the -60 kV SAPS event is 30%, compared to 19% for the -20 kV and 24% for the -40 kV case.

This dependence on SAPS potentials is seen in Figure 4, which shows the total ion density as a function of altitude at 21 MLT and $\lambda = 55°$. It can be seen that applying a SAPS potential of -20 kV resulted in a decrease in N_mF_2 of 25% whilst increasing H_mF_2 by 25 km. Similarly, applying a SAPS potential of -40 kV resulted in a decrease in N_mF_2 of 30% whilst increasing H_mF_2 by 40 km. Applying a potential of -60 kV resulted in the increase in H_mF_2 by 60 km whilst decreasing N_mF_2 by 38%.

The dominant ion in the F-region is O^+, which is converted into NO^+ and O_2^+ through the chemical reactions

$$O^+ + N_2 \rightarrow NO^+ + N \qquad (1)$$

and

$$O^+ + O_2 \rightarrow O_2^+ + O. \qquad (2)$$
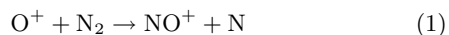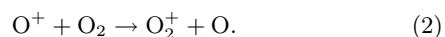
Previous work into the effects of northward directed electric fields Schunk et al. [1975] has shown that NO^+ can become the dominant ion in the F-region, however the electric field strengths used were an order of magnitude larger than those used in this study. The rate of conversion depends on the rate coefficients for these reactions and the concentration of N_2 and O_2. The rate coefficients are dependent on the effective temperature, defined as

$$T_{eff} = \frac{2}{3k_B} KE_{cm}, \qquad (3)$$

where KE_{cm} is the centre-of-mass kinetic energy [McFarland et al. [1973]]. The effective temperature can be obtained by

$$KE_{eff} = T_n + \frac{M_n}{M(O^+) + M_n} \times \left(\frac{M(O^+)}{3k_B} |\vec{v}_i - \vec{v}_n|^2 + T_i - T_n \right), \qquad (4)$$

where masses of the neutral and O^+ is given by M_n and $M(O^+)$ respectively and $\vec{v}_i - \vec{v}_n$ is the relative ion-neutral
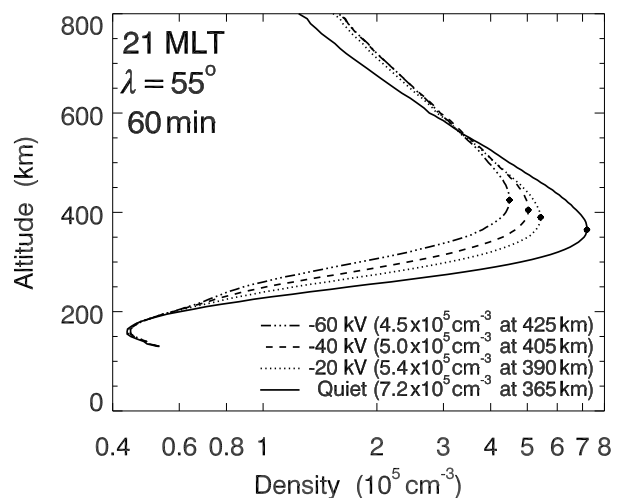

Figure 4. Total ion density as a function of altitude. N_mF_2 and H_mF_2 are plotted (dots) and shown in the legend for quiet conditions and SAPS potentials of -20, -40 and -60 kV events
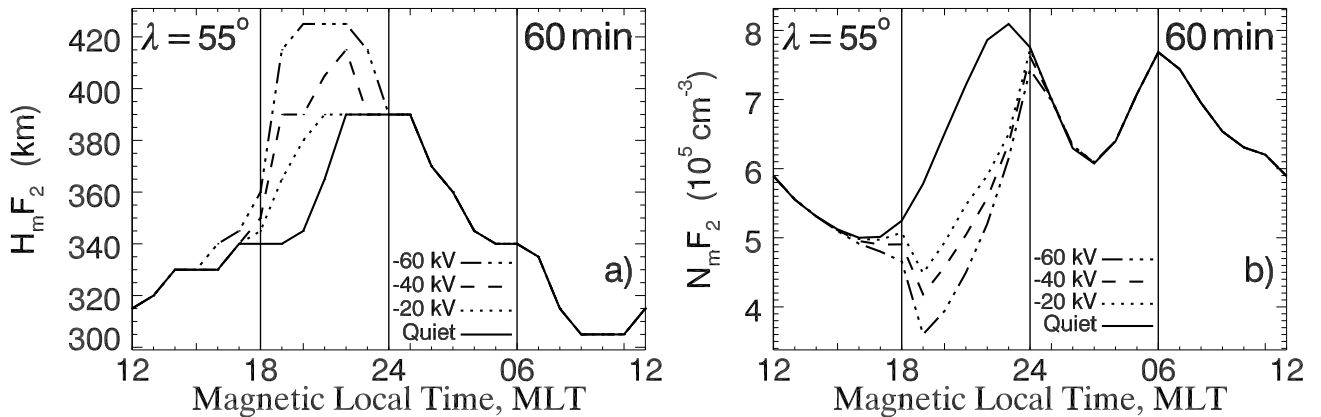
Figure 5. The variation in H_mF_2 and N_mF_2 with MLT after 60 min at $\lambda = 55°$ with various SAPS potentials

velocity. The effective temperature increases rapidly when the ion temperature T_i is raised significantly more than the neutral temperature T_n [McFarland et al. [1973]; Schunk et al. [1975]]. The increase in ion temperature due to the ion-neutral friction will thus increase the reaction rate, decreasing $[O^+]$ whilst increasing $[N_2^+]$ and $[O_2^+]$.

Ion densities above 600 km also increased during a SAPS and it was found that the increase is independent of SAPS potential. We suggest that this is due to the added ion-neutral frictional heating being kept constant for all three SAPS potentials resulting in similar thermal diffusion rates along the magnetic field lines above the F-region. The increase in Joule heating also plays a role in reducing the total ion density at F-region altitudes. Joule heating is the frictional heating of the neutral gas due to a difference in velocity between ions and neutrals. The Joule heating rate W in the frame of reference of the plasma is given by Vasyliunas and Song [2005].

$$W = \mathbf{J} \cdot \mathbf{E}' = \mathbf{J} \cdot (\mathbf{E} + (\mathbf{v}_n \times \mathbf{B})), \qquad (5)$$

where $\mathbf{v}_n$ is the velocity of the neutrals, $\mathbf{J}$ is the electric current, $\mathbf{E}$ is the electric field imposed on the ions and $\mathbf{B}$ is the magnetic field. An increase in Joule heating causes significant upwelling of the neutral air [Quegan et al. , 1992]. This results in an increase in N_2 and O_2 concentrations in the F-region which leads to an increase in the rate of conversion of O^+ ions into molecular ions (see Equations 1 and 2). Sellek et al. [1992] found that increased ion temperatures due to ion-neutral friction resulted in large upward field aligned velocities above the F-region whilst increased vertical velocities of the neutrals (due to Joule heating) caused minor increases in the ion field aligned velocity. Such flows have the added effect of lifting O^+ to higher altitudes with lower N_2 and O_2 densities and slowing the rate of conversion of O^+ into molecular ions. According to Anderson et al. [1991], vertical transport are more important for depleting the lower F-region than the fast chemistry at least at later development of the processes.

Figures 5a and 5b show the effects of the three SAPS potentials on H_mF_2 and N_mF_2 as a function of MLT at $55°$ magnetic latitude respectively after each simulation was run for 60 min. The height of the F_2-layer increases and the ion density at H_mF_2 decreases where SAPS is present, and the rate of the change is larger for stronger SAPS potential. Both the rise of H_mF_2 and the fall of N_mF_2 can reach 20 % for 60 kV SAPS at the centre of the SAPS MLT-region. At high F-region altitudes (above about 350 km), the scale height in the thermosphere can be several tens of km and hence the vertical grid spacing is relatively coarse compared to that used in the plasmasphere codes. This

has a knock-on effect on the coupling of the thermospheric and plasmaspheric models, and also on the smoothing algorithms used, resulting typically in plateau-like artifacts such as those seen in Figure 5a around 390 km). Significant influence of SAPS on H_mF_2 or on N_mF_2 after 24 MLT, where the SAPS is not present anymore, cannot be found, which may indicate weak transport effects.

Figures 6a and 6b show the effect of the various SAPS potentials on N_mF_2 as a function of time at 21 MLT and 23 MLT, respectively. Both show an initial sharp decrease in N_mF_2 followed by a more gradual reduction. The two hour presence of 60 kV SAPS can result in a drop of ion density more than 30 %. After the SAPS potential has been removed (at $t = 120$ min, indicated by the vertical line), there is a sharp increase in N_mF_2, followed by a slow return to the quiet simulation profile. The decrease of N_mF_2 at 23 MLT seems not only to slow down but even to reverse and increase after 90 minutes for all the three SAPS potentials. This phenomenon may be caused by transport effects. A more extensive statistical analysis could provide a more complete explanation in a future work.

To analyse the relative importance of the different processes contributing to the effects of SAPS in the ionosphere, we consider five cases labelled A to E. Profile A is a quiet-time run without any SAPS effect. Profile B is as per profile A, but with a -40 kV SAPS potential applied as described previously. However, the Joule heating in the thermosphere is artificially maintained at quiet-time levels. Profile C is as per profile B, except that we permit the Joule heating to vary self-consistently with the applied potential. Profile D is as per profile C, except that we add an increase in the effective temperature due to increased relative ion-neutral velocities; we use the ion temperature given by the extended TTM model as per Figure 2a. Finally, profile E is as per profile D, except that we further add a temperature profile corresponding to ion-neutral heating, as per Figure 2b. Hence, profile A and profile E correspond to a quiet run and to a run with -40 kV SAPS, respectively, displayed in Figures 6a and 6b., while profiles B, C and D are 'transitional' cases, in the sense that they represent only partial effects (convection, Joule heating, effective temperature enhanced by ion-neutral velocity) of a SAPS event only.

Figures 7a and 7b show the temporal variation of N_mF_2 at 21 MLT and 23 MLT, respectively, for $\lambda = 55°$. During the first 120 min of the -40 kV SAPS event, it can be seen that the westward convection of flux tubes (see profile B) increases N_mF_2 at 21 MLT and decreases it at 23 MLT relative to the quiet results (profile A). Profile C shows that Joule heating leads to a substantial decrease in N_mF_2. This is due to the enhanced concentration of N_2 and O_2 in the F-region due to the upwelling of the thermosphere. Profile D
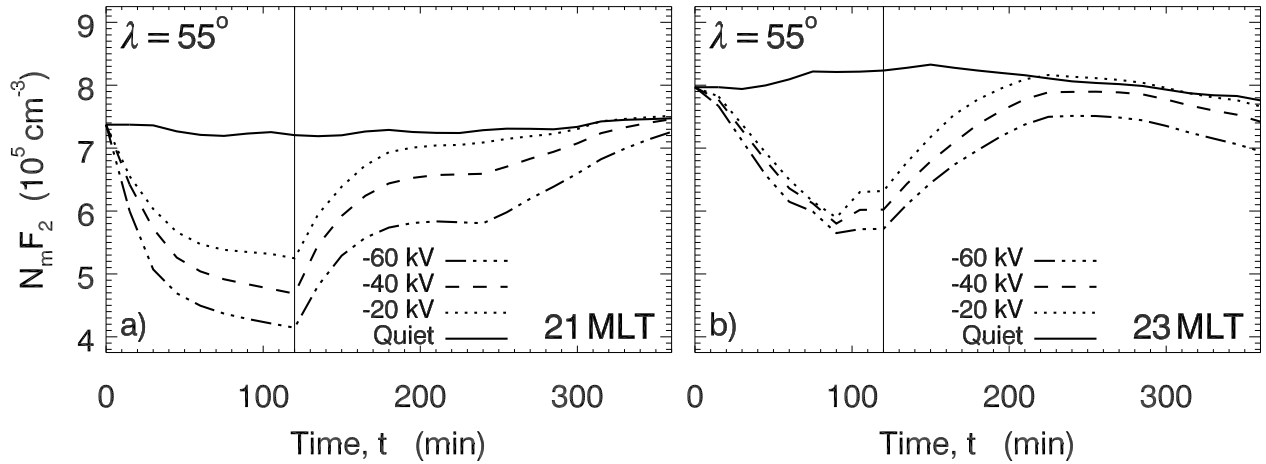
Figure 6. Effects of the various SAPS potentials on N_mF_2 as a function of time at 21 and 23 MLT and 55° λ.
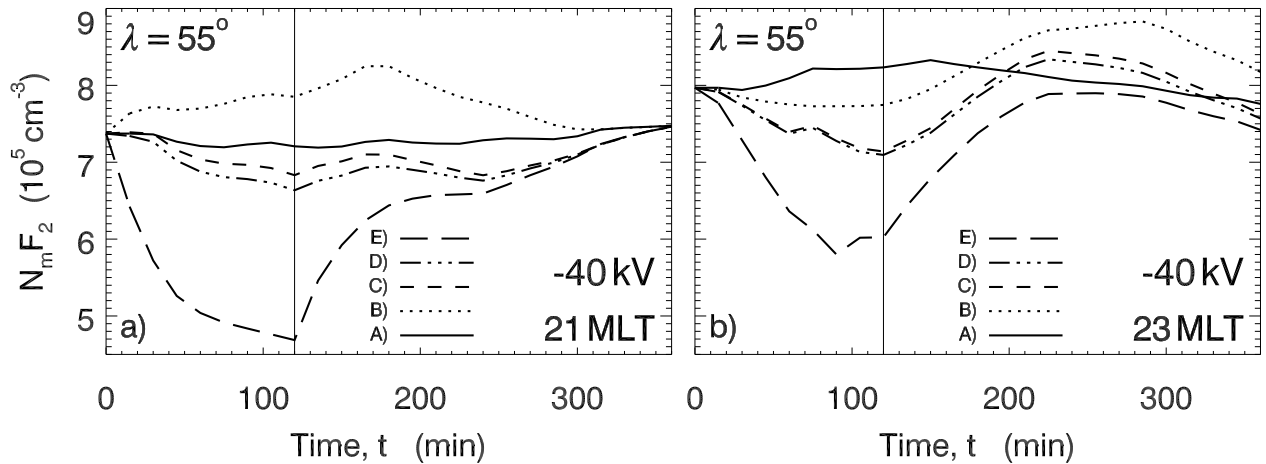

Figure 7. N_mF_2 as a function of time. The individual processes have been isolated A) Quiet time run (0 kV) B) -40 kV with only convection included C)-40 kV with convection and Joule heating D) -40 kV with TTM (convection and Joule heating included) E) -40 kV with TTM + ion-neutral friction (convection and Joule heating included)

shows that the increase in relative ion-neutral velocity due to the $E \times B$ drift has the least effect on N_mF_2 in comparison to the effects that convection, Joule heating and ion-neutral friction has. Profile E shows the most change in N_mF_2 with sharp decreases at both 21 MLT and 23 MLT as soon as the SAPS event begins. The heating due to ion-neutral friction has two effects on the F-region. Firstly, the large increase in effective temperature results in increased recombination of O^+. Secondly, the increase in ion temperature leads to increased field aligned velocities, forcing the F-region to higher altitudes. Diffusion along the field lines due to increased ion temperatures has already been shown (at the discussion of Figure 4 and reference to Sellek et al. [1992]) to result in increased total ion density at altitudes above 600 km. After the presence of SAPS (switched off at $t = 120$ min), the recovery phase starts, which lasts for around two hours. Without taking into account the temperature increase due to ion-neutral friction, an overshoot of N_mF_2 can occur in the second hour of the recovery phase at 23 MLT (profiles B, C and D in Figure 7a). However, N_mF_2 for profile D, which represents the complete SAPS effect, does not exceed the value for the quiet run (i.e., that for profile A) We conclude that ion-neutral friction is an important effect in

SAPS, serving to increase the ion temperature and thus the O^+ loss rate, and hence suppressing N_mF_2.

The effect of the various SAPS potentials on H_mF_2 as a function of time is shown in Figure 8a for 21 MLT and Figure 8b for 23 MLT. (Notice that from now on the complete SAPS effect is studied, i.e., with convection, Joule heating, and enhanced effective temperature wich includes the extended TTM and ion-neutral friction.) Results show that at 21 MLT, H_mF_2 increases as soon as the SAPS potential is applied whilst at 23 MLT, the increase in H_mF_2 is delayed by 60 min for the -60 kV events and by 90 min for the -20 kV and -40 kV events. When the SAPS potential is removed at $t = 120$ min, at 21 MLT all three SAPS events return to quiet time values quickly whilst at 23 MLT there is a 30 min delay before returning. (The steps in the H_mF_2 vs. time graphs, in Figure 8, are due to the relatively poor vertical spatial resolution along the magnetic field lines around H_mF_2.).

Figure 9 shows the temporal variation of VTEC at 21 MLT and 23 MLT for the different SAPS events. At 21 MLT, VTEC drops rapidly for around an hour before flattening off to a minimum when the SAPS is removed at $t = 120$ minutes. Subsequently, there is a rapid recovery lasting around an hour before a maxima at $t \approx 190$ minutes,
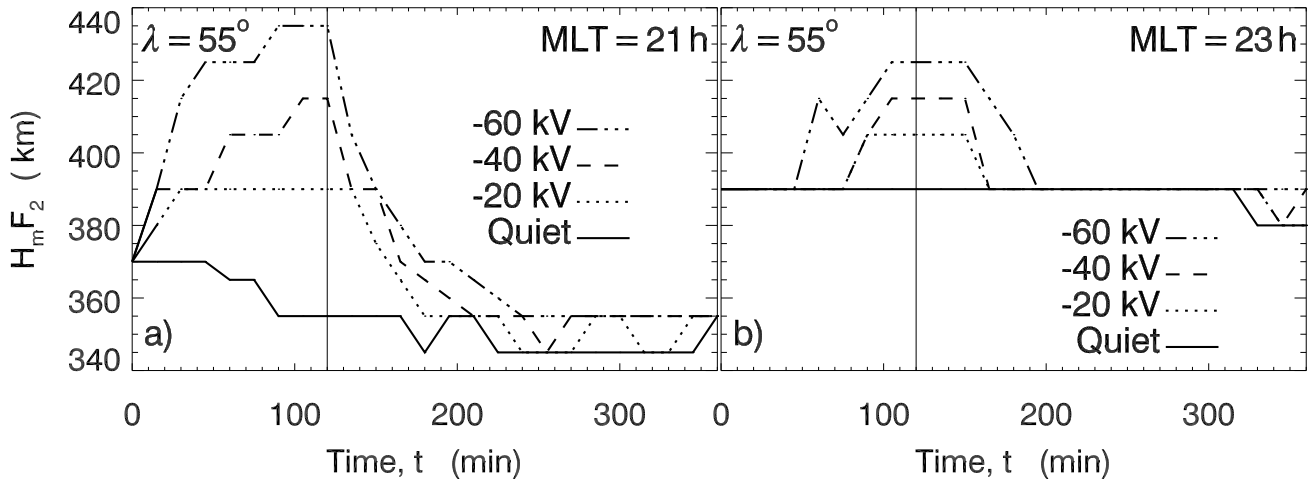
Figure 8. Effects of the various SAPS potentials on H_mF_2 as a function of time at 21 MLT and 23 MLT and 55° λ.
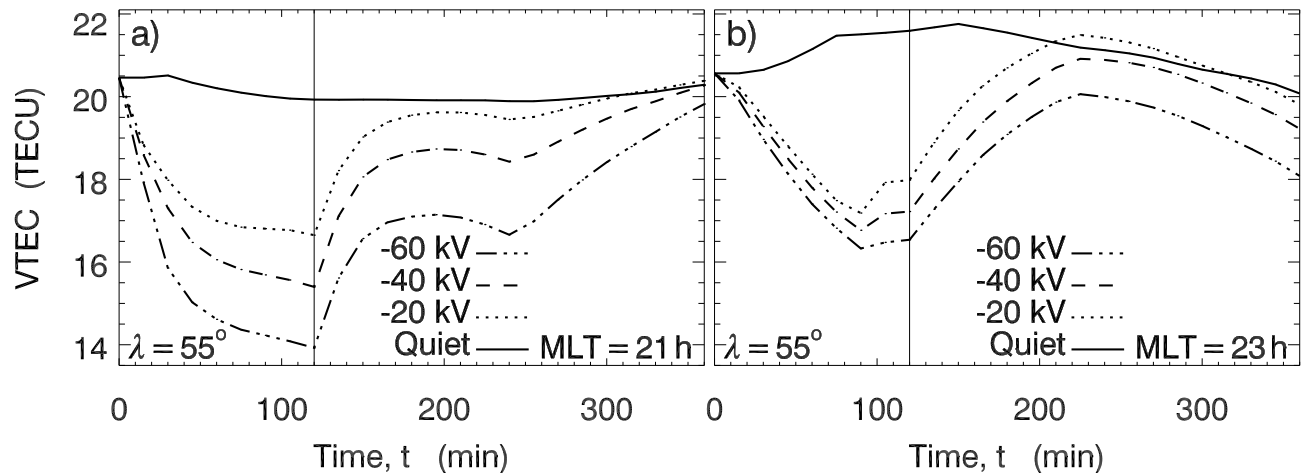

Figure 9. Effects of the various SAPS potentials on VTEC as a function of time at 21 MLT and 23 MLT and 55° λ.

followed by another small drop to a secondary minimum at $t \approx 240$ minutes. There then follows a recovery to quiet-time levels for t > 360 minutes. At 23 MLT the behavior is less complex. The initial drop is approximately linear until $t \approx 100$ minutes, when there is a small recovery; when the SAPS is removed at $t = 120$ minutes, the recovery to approximately quiet-time levels lasts until $t \approx 220$ minutes, after which VTEC tracks the quiet-time level.

The broad behaviour - an intial decrease in VTEC due to rapid recombination, followed by a recovery after the removal of the SAPS - has been discussed previously, and is expected.

In the 21 MLT case, we see a secondary minimum at $t \approx 240$ minutes, i.e., two hours after the removal of the SAPS. If this is a feature corotating onto 21 MLT, it would correspond to the feature being located at 19 MLT at the time the SAPS is turned off. This feature is difficult to explain. In the -60 kV SAPS case, this location corresponds closely (within the resolution of the model) with that of plasma which started at 24 MLT at $t = 0$ (i.e., the eastward SAPS boundary), and undergoing a strong westward $E \times B$ drift overcoming a weak eastward co-rotation. (In the 23 MLT case, there is a suggestion of a very weak secondary minimum at $t \approx 360$, not shown; if this is the same feature as in the 21 MLT case, it lends credence to the corotation theory). However, this minimum is also present, albeit weakly so, in the 40 kV and 20 kV SAPS cases where the $E \times B$ drift is much weaker, which suggests the pres-

ence of a feature unrelated to the SAPS. The terminator would take 3 hours to corotate onto 21 MLT, arriving at $t = 300$ minutes rather than the 240 minutes indicated; however, the relatively coarse (18°) longitudinal resolution of the flux tube groups, together with the associated smoothing scheme, makes this the most likely candidate. A future version of CTIP with higher resolution flux tube groups would enable this feature to be studied in detail.

A feature visible in the 23 MLT case but not in the 21 MLT case is the shoulder/start of recovery between $t = 100$ and $t = 120$ minutes. An increase in VTEC cannot simply be vertical transport rearranging the plasma within the F-region (as might have explained the similar feature seen in N_mF_2, Figure 7b profile E), so we are seeing either horizontal transport of plasma, or altered chemistry. Again, the time synchronicity of the events suggests that it is unrelated to the $E \times B$ drift. We cannot convincingly explain this feature.

The long-term recovery of the SAPS can be studied in the 23 MLT case, unaffected by the (possible) corotating terminator. The -20 kV and -40 kV cases recover to within a few percent of quiet time levels around $t = 220$ minutes (i.e., around 100 minutes after the SAPS is removed). However, the -60 kV SAPS case exhibits a marked hysteresis with the recovery falling short of the quiet time VTEC by about 10%. We suggest that this behaviour is due to the stronger $E \times B$ drifts driving a thermospheric 'flywheel' that forces plasma semi-permanently from the region due to Coriolis forcing.

To study the recovery time without the influence of corotation, N_mF_2 of a flux tube in a Lagrangian reference frame (i.e., an individual flux-tube is followed) is given in Figure 10 after the SAPS event has ceased. Once the SAPS potential is removed, a single flux-tube is followed from 23 MLT and $55°$ λ for 10 hours as it corotates with the Earth. The flux-tube travels from the pre-midnight sector (23 MLT) to the pre-noon sector (09 MLT), arriving at $t = 720$ min. The percentage difference between the N_mF_2 affected by a SAPS event and the quiet simulation is plotted in Figure 10. The N_mF_2 of the flux tube is reduced by 20% to 30% by the end of the two hour of present of SAPS. The 'recovery time' can be defined as the time taken to recover to within 5% of the pre-SAPS density. As can be expected, the stronger the SAPS potential field is the longer recovery time is needed. The -20 kV SAPS takes 2 h to recover to within 5% of its 'quiet-time' value, the -40 kV SAPS takes 3 h and the -60 kV SAPS takes about 3.5 h.

5. Conclusion

Electrostatic potentials of -20, -40 and -60 kV were imposed on the pre-midnight region, 18 to 24 MLT, equatorward of the plasmaspheric footprints, $50°$ to $60°$ λ to simulate sub-auroral polarization streams (SAPS). The response of the ionosphere to a 2 h presence of SAPS was investigated by studying the resulting VTEC, N_mF_2 and H_mF_2 profiles. The ion density in the F-region decreases rapidly once a SAPS potential is imposed and that the decrease is larger for increasing SAPS potentials. This decrease is due to the rapid conversion of O^+ into NO^+ and O_2^+ through chemical reactions with N_2 and O_2 respectively, and the subsequent fast recombination. The recombination rates of both chemical reactions are dependent on the ion temperature which increases due to the ion-neutral frictional heating and also on the concentration of N_2 and O_2 which increases in the F-region due to the enhanced Joule heating of the thermosphere.

There is also an increase in H_mF_2 when a SAPS potential is imposed. The height can increase by up to 80 km for a SAPS potential of -60 kV. The increased ion temperatures during a SAPS event leads to greater diffusion along the magnetic field lines resulting in an increase in ion densities at some height above H_mF_2.

VTEC also sharply decreases when a SAPS potential is imposed, by 30% during a -60 kV SAPS event. When the SAPS potential is removed N_mF_2, H_mF_2 and VTEC return to quiet simulation values within 2 to 4 hours, depending on the strength of the SAPS potential.

It would be a great step forward to study the possible latitudinal distribution and the actual temporal evolution of observed SAPS events. Based on that, a more realistic SAPS electric field should be constructed to represent the SAPS events, and by that a more realistic picture could be obtained about the evolution of the ionosphere during and after sub-auroral polarization streams.

References

Anderson, P.C., R.A. Heelis, and W.B. Hanson (1991), The ionospheric signatures of rapid subauroral ion drifts, *J. Geophys. Res.*, *96* (A4), 5785-5792. Multisatellite observations of rapid subauroral ion drifts (SAID)

Anderson, P.C., D.L. Carpenter, K. Tsuruda, T. Mukai and F.J. Rich (2001), Multisatellite observations of rapid subauroral ion drifts (SAID), *J. Geophys. Res.*, *106* (A12), 29585-29600.

Burke, W.J., Rubin, A. G.; Maynard, N. C.; Gentile, L. C.; Sultan, P. J.; Rich, F. J.; de La Beaujardire, O.; Huang, C. Y.; Wilson, G. R. (2000), Ionospheric disturbances observed by DMSP at middle to low latitudes during the magnetic storm of June 4-6, 1991, *J. Geophys. Res.*, *105* (A8), 18391-18406.

Foster, J.C., and W.J. Burke (2002), SAPS: A new characterization for sub-auroral electric fields, *EOS*, *83*, 393-394.

Foster, J.C., and H.B. Vo (2002), Average characteristics and activity dependence of the subauroral polarization stream, *J. Geophys. Res.*, *17* (A12), 1475, doi:10.1029/2002JA009409.

Fuller-Rowell, T.J., and D. Rees (1980), A three-dimensional time-dependent global model of the thermosphere, *J. Atmos. Sci*, *37*, 2545-2567.

Gal'Perin, Y.I., V.N. Ponomarev, and A.G. Zosimova (1973), Direct Measurements of Drift Rate of Ions in Upper Atmosphere during a Magnetic Storm. II. Results of Measurements during Magnetic Storm of November 3, 1967, *Cosmic Research*, *11*, 249-258.

McFarland, M., D.L. Albritton, F.C. Fehsenfeld, E.E. Ferguson, and A.L. Schmeltekopf (1973), Flow-drift technique for ion mobility and ion-molecule reaction rate constant measurements. II. Positive ion reactions of NO^+, O^+, and H with O_2 and O^+ with N_2 from thermal to 2 eV, *J. Chem. Phys.*, *59* (12), 6620-6628.

Millward, G.H., R.J. Moffett, S. Quegan, and T.J. Fuller-Rowell (1996), A coupled thermosphere-ionosphere-plasmasphere model (CTIP), in STEP Handbook on Ionospheric Models, edited by R.W. Schunk, pp. 239-279, Utah State University, Logan.

Moffett, R.J., R.A. Heelis, R. Sellek, and G.J. Bailey (1992), The temporal evolution of the ionospheric signatures of subauroral ion drifts, *Planetary and Space Science*, *40* (5), 663-670.

Quegan, S., G.H. Millward, and T.J. Fuller-Rowell (1992), A study of the evolution of a high latitude trough using a coupled ionosphere/thermosphere model, *Advances in Space Research*, *12* (6), 161-169.

Schunk, R.W., P.M. Banks, and W.J. Raitt (1975), Effect of electric fields on the daytime high-latitude E and F regions, *J. Geophys. Res.*, *80*, 3121-3130.

Sellek, R., G.J. Bailey, R.J. Moffett, R.A. Heelis, and P.C. Anderson (1991), Effects of large zonal plasma drifts on the sub-auroral ionosphere, *Journal of Atmospheric and Terrestrial Physics*, *53* (6-7), 557-565.

Sellek, R., R.J. Moffett, and G.J. Bailey (1992), Effects of rapid zonal plasma flow in the mid-latitude ionosphere: Modulation of the field-aligned plasma flow by neutral air upwelling, *Advances in Space Research*, *12* (6), 171-174.

Smiddy, M., M.C. Kelley, W.J. Burke, F. Rich, R. Sagalyn, B. Schman, R. Hays, and S. Lai (1977), Intense poleward-directed electric fields near the ionospheric projection of the plasmapause, Geophys. Res. Lett., 4, 543-546

Spiro, R.W., R.A. Heelis, and W.B. Hanson (1979), Rapid subauroral ion drifts observed by Atmospheric Explorer C, *Geophys. Res. Lett.*, *6*, 660-663.

Titheridge, J.E. (1998), Temperatures in the upper ionosphere and plasmasphere, *J. Geophys. Res*, *103* (A2), 2261-2277.

Vasyliunas, V.M., and P. Song (2005), Meaning of ionospheric Joule heating, *J. Geophys. Res.*, *110*, A02301, doi:10.1029/2004JA010615.

Webb, P.A., and E.A. Essex (2003), Modifications to the Titheridge upper ionosphere and plasmasphere temperature model, *J. Geophys. Res*, *108* (A10), 1359.

Yeh, H., -C., J.C. Foster, F.J. Rich, and W. Swider (1991), Storm-time electric field penetration observed at mid-latitude, *J. Geophys. Res.*, *96*, 5707-5721.

B. Pintér, Department of Applied Mathematics, The University of Sheffield, Hicks Building, Sheffield, S3 7RH, UK. (b.pinter@sheffield.ac.uk)
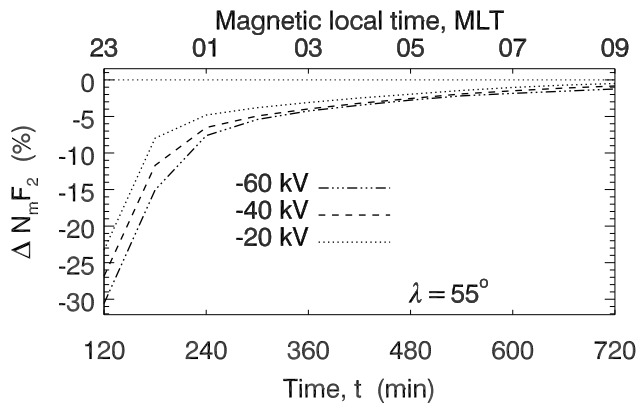
Figure 10. N_mF_2 as a function of time following a flux tube from t=120 min (when the SAPS electric field is removed) at 23 MLT as it corotates for 10 hours and reaches 09 MLT